J Physiol 587.4 (2009) pp 769–785

The Journal of Physiology

Neuronal oscillations and the rate-to-phase transform: mechanism, model and mutual information

Douglas McLelland and Ole Paulsen

Department of Physiology, Anatomy and Genetics, University of Oxford, Oxford, UK

Theoretical and experimental studies suggest that oscillatory modes of processing play an important role in neuronal computations. One well supported idea is that the net excitatory input during oscillations will be reported in the phase of firing, a 'rate-to-phase transform', and that this transform might enable a temporal code. Here, we investigate the efficiency of this code at the level of fundamental single cell computations. We first develop a general framework for the understanding of the rate-to-phase transform as implemented by single neurons. Using whole cell patch-clamp recordings of rat hippocampal pyramidal neurons *in vitro*, we investigated the relationship between tonic excitation and phase of firing during simulated theta frequency (5 Hz) and gamma frequency (40 Hz) oscillations, over a range of physiological firing rates. During theta frequency oscillations, the phase of the first spike per cycle was a near-linear function of tonic excitation, advancing through a full 180 deg, from the peak to the trough of the oscillation cycle as excitation increased. In contrast, this relationship was not apparent for gamma oscillations, during which the phase of firing was virtually independent of the level of tonic excitatory input within the range of physiological firing rates. We show that a simple analytical model can substantially capture this behaviour, enabling generalization to other oscillatory states and cell types. The capacity of such a transform to encode information is limited by the temporal precision of neuronal activity. Using the data from our whole cell recordings, we calculated the information about the input available in the rate or phase of firing, and found the phase code to be significantly more efficient. Thus, temporal modes of processing can enable neuronal coding to be inherently more efficient, thereby allowing a reduction in processing time or in the number of neurons required.

(Received 29 September 2008; accepted after revision 15 December 2008; first published online 22 December 2008)
Corresponding author D. McLelland: Department of Physiology, Anatomy and Genetics, University of Oxford, Oxford, UK. Email: douglas.mclelland@dpag.ox.ac.uk

A fundamental question in neuroscience is the nature of the neural code. How, precisely, do neurons represent and transmit information? Action potentials, or 'spikes', are the presumed building blocks of the code, but controversy remains as to the details of the code itself (Rieke *et al.* 1997). In the eight decades since Adrian described the trains of pulses in frog nerves generated in response to muscle stretch (Adrian, 1926), ideas of a code based on the average number of spikes in a given time interval have dominated, the so-called *rate code*. Throughout, however, neuroscientists have been aware that the precise timing of spikes might also encode information, a *temporal code*.

Theoretically, a temporal code would have the potential to efficiently and rapidly transmit information (Gautrais & Thorpe, 1998) and support useful computations (Hopfield, 1995). However, there has been a relative paucity of strong experimental evidence of a temporal code in recordings of neuronal activity, and the biophysical ability of individual neurons to generate patterns of action potentials with sufficient temporal precision has been questioned. Recently, however, it has become increasingly clear that precise temporal patterns of spiking activity (with properties not trivially intrinsic to the stimulus) can indeed be recorded from neurons at all levels, from early sensory input (e.g. somatosensory afferents; Johansson & Birznieks, 2004) to the highest cortical levels (e.g. place cell phase precession in the rodent hippocampus; O'Keefe & Recce, 1993). Moreover, it has been demonstrated that individual neurons are capable of generating precisely timed, repeatable patterns of activity, provided they are driven by fluctuating rather than purely tonic input (Bryant & Segundo, 1976; Mainen & Sejnowski, 1995; Schaefer *et al.* 2006).

In order for a temporal code to operate, a temporal reference is required. A good candidate for this is oscillatory activity, which is prevalent in the cortex and

DOI: 10.1113/jphysiol.2008.164111

could provide a common reference both within local circuits and across cortical areas.

The best-studied example of an oscillation-based temporal code is hippocampal phase precession in rodents. When a rodent explores an environment, prominent theta frequency oscillations (4–12 Hz) are seen in the hippocampus. Also, individual cells in the hippocampus, place cells, are seen to fire in restricted areas of the environment, their place fields. As an animal traverses a neuron's place field, the phase of firing advances relative to the ongoing theta frequency oscillation (O'Keefe & Recce, 1993). In fact, in reconstructing an animal's position from neuronal activity, using phase information substantially improves the accuracy over that estimated from firing rate alone (Jensen & Lisman, 2000).

What mechanisms control the phase of firing of individual neurons? One attractive possibility, which has been implemented in theoretical models, is based on a simple rate-to-phase transform (Hopfield, 1995), in which the phase of firing advances with increasing tonic input. Electrophysiological studies have suggested that a transform of this nature could indeed be implemented by neurons (Kamondi *et al.* 1998; Magee, 2001; Harris *et al.* 2002; Mehta *et al.* 2002; Margrie & Schaefer, 2003) but have not explored the basis for this transform.

Here, we take advantage of the precise experimental control of neuronal input afforded by the whole-cell patch clamp set-up in the *in vitro* brain slice to examine the properties of the rate-to-phase transform in hippocampal pyramidal neurons. A simple mathematical description of this transform is presented, allowing generalization to other types of neurons and oscillations. Finally, we estimate the mutual information of the transform based on the experimentally observed temporal precision.

Methods

Slice preparation

Horizontal hippocampal slices (300 μm) were prepared from a total of 29 juvenile Wistar rats (P13–P19), following decapitation under deep isoflurane-induced anaesthesia, in accordance with UK Home Office regulations. Slices were maintained at room temperature in a submerged-style holding chamber until transferred one by one to the recording chamber and superfused with artificial cerebrospinal fluid at 30°C, containing (mM): NaCl 126; KCl 3; NaH_2PO_4 1.25; $MgSO_4$ 2; $CaCl_2$ 2; $NaHCO_3$ 24; glucose 10; pH 7.2–7.4; and bubbled with carbogen gas (95% O_2, 5% CO_2).

Recordings

Whole-cell patch clamp recordings were made from pyramidal cells in area CA1, under visual guidance using infrared differential interference contrast video microscopy. Patch pipettes (serial resistance 5–10 MΩ) were pulled from standard-walled borosilicate capillary tubing (GC120F-10, Harvard Apparatus, Edenbridge, UK). Electrode solution contained (mM): potassium gluconate 110; Hepes 40; NaCl 4; ATP-Mg 4; GTP 0.3; with 5 mg ml^{-1} biocytin included for consistency with other studies; pH was adjusted to 7.4 using KOH (1 M).

Current clamp recordings were made using Axoclamp 2B or Multiclamp 700A amplifiers (Axon Instruments, Union City, CA, USA). Capacitance was fully compensated, and bridge balance monitored and adjusted throughout (18–35 MΩ). Measured voltages were corrected for the liquid–liquid junction potential of −15.5 mV, calculated using the built-in function of pCLAMP (Axon Instruments) (Ng & Barry, 1995). The voltage signal was low-pass filtered at 1 kHz or 3 kHz, using the built-in Bessel filters of the amplifiers, before being digitally converted using ITC-16 or ITC-18 A/D boards (Instrutech Corp., Port Washingon, NY, USA) and acquired online at 4 kHz (for 1 kHz filtered input signals) or 8 kHz (for 3 kHz filtered input signals). Dynamic clamp was implemented using an ITC-18 A/D board (Instrutech).

All current clamp and dynamic clamp command signals were generated, and data acquired and analysed using Igor Pro software (Wavemetrics, Lake Oswego, OR, USA).

Recording protocols

We applied a range of levels of tonic excitatory current, with or without a sinusoidally modulated current or conductance, as described in Results. The order of presentation of different levels of excitatory current was randomised, and at each level oscillatory and oscillation-free trials were interleaved, with each condition repeated 5 times. Tonic excitatory current steps lasted 3 s, but only the latter 2 s were analysed, in order to avoid the rapidly adapting response to step onset (typically, a CA1 pyramidal neuron *in vivo* shows a fairly gradual rise and fall in firing rate as the animal traverses the place field of that cell, O'Keefe & Recce, 1993; Skaggs *et al.* 1996). To avoid the build-up of slow adaptive responses to prolonged excitation, there was a 2 s rest period between trials. This period also enabled us to monitor the baseline state of cells, to ensure stability over the course of recording.

We tested a range of inputs which yielded firing rates approximately matching those recorded *in vivo* (see, e.g. O'Keefe & Recce, 1993).

Analyses

Linear fits to the firing rate in response to tonic input alone (the 'oscillation-free' firing rate) were used as a measure of cell activation for that level of input. When this value

was used as the independent variable for quantification of other variables, it provided satisfactory normalization across cells (see Fig. 1*B* and *C*). Because linear fits to the *f–I* curves were used, values can be extrapolated into 'negative' firing rate ranges, allowing the inclusion of responses to levels of input which, although subthreshold in the case of the oscillation-free input, did generate spikes when in combination with oscillatory currents.

Instantaneous input resistance and membrane time constant at resting potential were estimated from exponential fits to the initial 10–20 ms of membrane potential response to repeated (> 20) brief hyperpolarizing current pulses.

Phase values are reported in degrees, with 0 deg taken as the peak of the sinusoidal current input.

Use of non-circular statistics

In analysing phase data, it is often necessary to use circular statistics. However, while the circular mean can

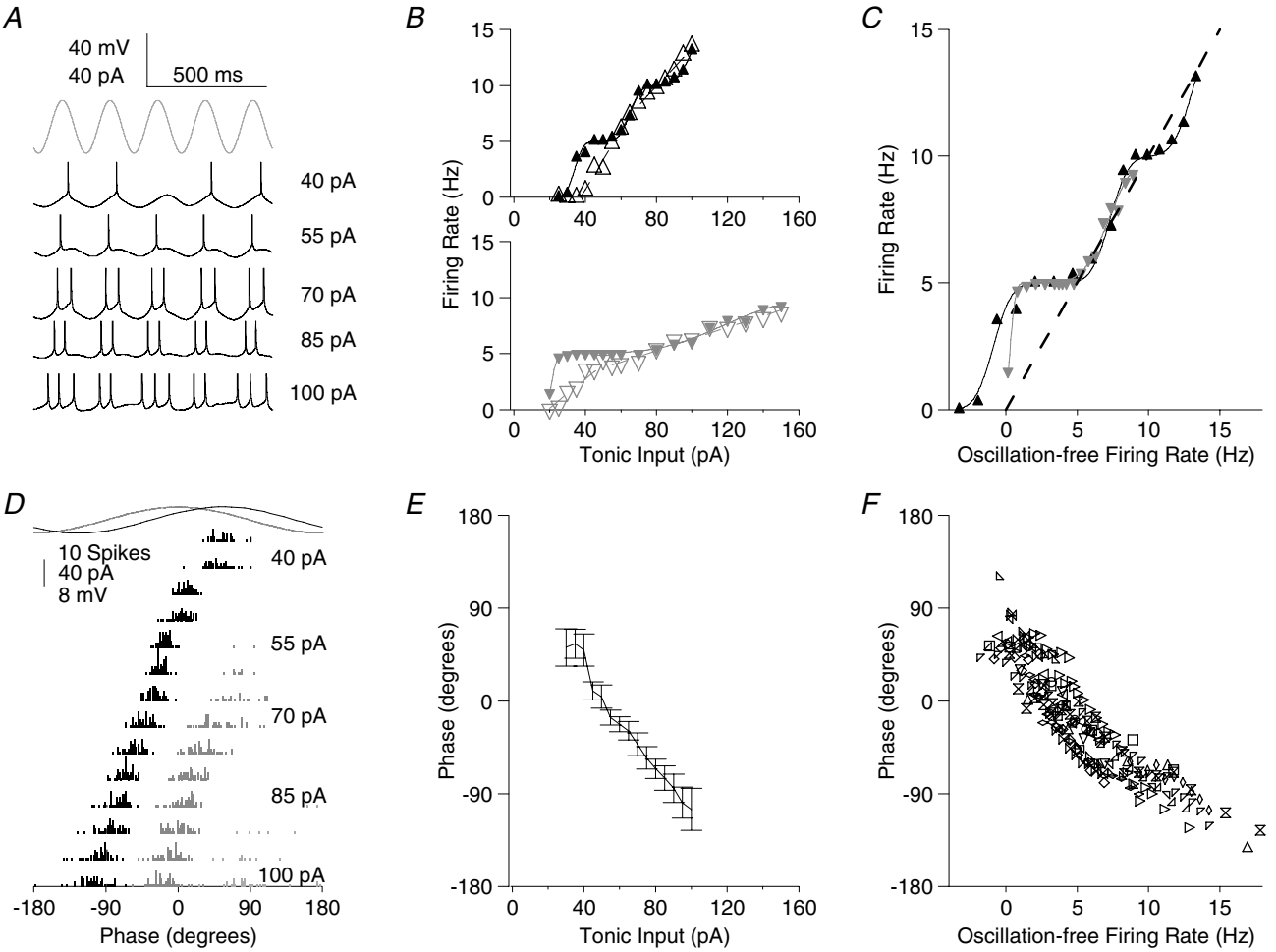

Figure 1. Phase of firing relative to theta frequency sinusoidal current is dependent on the level of tonic excitation

A, membrane potential traces for a typical cell receiving a fixed amplitude of theta frequency (5 Hz) sinusoidal current input (trace indicated in grey at the top for comparison of timing) and a range of levels of tonic depolarizing current (indicated to the right of the traces). Spikes are truncated at –20 mV for clarity. *B, f–I* curve for two typical cells, with (filled symbols and lines) and without (open symbols and dashed lines) sinusoidal theta frequency current. As is apparent in *A*, firing tends to lock to the oscillatory input, yielding plateaux in the *f–I* curve at firing rates equal to integer multiples of the oscillation frequency. *C, f–I* curves for the two cells shown in *B*, with normalization on the abscissa carried out by converting the tonic current input level to the firing rate induced in the absence of oscillatory input (see Methods). This method of normalization is used throughout for the presentation of pooled data. *D,* spike time histograms for the same cell as in *A*, relative to the oscillatory cycle, across the range of tonic input levels tested (first spike per cycle, black; second spike per cycle, dark grey; third spike per cycle, light grey). *E*, ϕ*–I* curve for the same cell (mean ± S.D.). *F*, scatter plot of mean firing phase *versus* oscillation-free firing rate for the population of cells.

be easily interpreted, further descriptive statistics do not provide the direct intuitive understanding of the underlying distributions that is provided by their non-circular equivalents (e.g. standard deviation). We therefore find it desirable to use non-circular statistics where possible. Additionally, this facilitates the description of probability distributions required for information theoretic estimates.

We justify the use of non-circular statistics in the present case, noting that for both theta and gamma frequency inputs, there was always a portion of the oscillation cycle during which virtually no spikes occurred (in the quadrant orthogonal to the circular mean phase of spikes, fewer than 0.05% of spikes occurred for the theta oscillation, and fewer than 2% of spikes occurred for the gamma oscillation). As such, spikes can be unambiguously assigned to a given oscillatory cycle (there is no confusion between late spikes in one cycle and early spikes in the following cycle). By choosing an appropriate range over which to express spike phase, the confounding circular wrap-around point can be avoided in calculation of the mean and variance. In support of this argument, the difference between normal and circular means was on average only 0.13 deg for theta oscillations and 0.37 deg for gamma oscillations.

Mutual information estimates

We estimated mutual information (Shannon, 1948) between the tonic input and either the rate of firing or the phase of firing (where theta frequency oscillatory input was included) or interspike interval (where no oscillatory input was included), according to the standard formula

$$I(R;S) = H(R) - H(R|S)$$

where $I(R; S)$ is the mutual information between response R and stimulus S; $H(R)$ is the entropy of the response; and $H(R \mid S)$ is the conditional entropy of response given the stimulus. We opted not to use our discrete data points in the calculation of these values, because of the bias inherent in that approach (Panzeri *et al.* 2007). Instead, we represented the responses as continuous functions of the stimulus based on our data, and applied the following formulae for calculation of the relevant entropy values, using notation as in Borst & Theunissen (1999):

$$H(R) = -\int_{R_{\min}}^{R_{\max}} p(r)\log_2 p(r)\,\mathrm{d}r$$

$$H(R|S) = -\int_{S_{\min}}^{S_{\max}} p(s)\int_{R_{\min}}^{R_{\max}} p(r|s)\log_2 p(r|s)\,\mathrm{d}r\,\mathrm{d}s$$

The stimulus distribution itself was assumed to be flat over the range of input values tested. While we do not believe that this is likely to reflect the reality in most physiological systems, this should not affect our conclusion, since for all codes studied, the distribution of information across stimulus values was very nearly flat. Hence, any skew in the distribution of stimulus values should have a similar effect on each of the codes.

For the phase code, experimentally obtained ϕ–I (mean phase–current) curves for each cell were fit by arccos functions of the tonic input current, as suggested by our analytical model, and the standard deviation at any given point on that curve estimated from the experimental data (assuming normally distributed phase values for any fixed level of tonic current; data were not significantly different from normal distributions, Kolmogorov–Smirnov test, $P > 0.1$). With regard to the rate code, the response is a discrete variable, viz. the number of spikes in a fixed interval (we used integer multiples of 200 ms, that is, 1 theta cycle, for direct comparison with the phase code). Since f–I curves were well fit by a series of cumulative Gaussian functions (one for each spike-per-cycle, see Fig. 1*B* and *C*), the requisite probability functions (one for each of the possible spike totals in the period of interest) were fit by difference-of-cumulative Gaussian functions. Regarding the interspike interval (ISI) code, we used the corresponding instantaneous spike frequency values (f_i) since these were linearly related to tonic current, allowing straightforward estimation of mutual information. Distributions of f_i values were not significantly different from normal distributions (Kolmogorov–Smirnov test, $P > 0.1$). Standard deviation of f_i was estimated, based on experimental recordings, as a decaying exponential function of tonic input, and the potential for multiple measurements of the ISI (three or more spikes in the relevant period) was taken into account.

Mutual information was estimated independently for each cell, and only over the range of inputs which had been specifically tested in that cell (i.e. we did not use estimated model parameters to extrapolate across the range of possible inputs).

Results

We first report data from CA1 pyramidal neurons recorded in current clamp mode ($n = 15$; mean resting potential on whole-cell access, $V_R = -73.7 \pm 1.9$ mV; membrane time constant, $\tau_m = 22.5 \pm 5.7$ ms; input resistance, $R_{in} = 142 \pm 36$ MΩ; mean ± S.D.).

In order to investigate the rate-to-phase transform in single neurons, we injected a combination of sinusoidally modulated current of fixed amplitude, and a range of levels of tonic excitatory current. Two frequencies of oscillatory current were tested: theta (5 Hz) and

gamma (40 Hz), both of which have been reported in the subthreshold membrane potential of hippocampal pyramidal cells, recorded *in vivo* in the anaesthetized rat (Soltesz & Deschênes, 1993; Kamondi *et al.* 1998). A sinusoidal current generated oscillations in the membrane potential approximating those described *in vivo* (5 mV peak-to-peak for theta; 2 mV peak-to-peak for gamma). In most cells, 40 pA peak-to-peak oscillatory current proved to be appropriate. In a few cells with higher membrane impedance, 30 or 20 pA was used. We tested the response of cells to the same range of tonic excitatory input levels in the presence and absence of oscillatory input.

Theta frequency input

The firing pattern of CA1 pyramidal cells in response to tonic current injection alone has been previously described (Lanthorn *et al.* 1984). Consistent with those results, the firing rate of the cells we recorded was a near-linear function of tonic current injection over a limited range, rising from an arbitrarily low value near threshold, consistent with Type I cell behaviour, and reaching a maximum near 20 Hz. Higher levels of current injection typically led to depolarization-block and deterioration of the cell.

In contrast, the frequency–current (*f–I*) curve in the presence of theta frequency sinusoidal input was strikingly non-linear, with distinct plateaux at firing rates equal to integer multiples of the oscillation frequency (Fig. 1*A* and *B*).

There was considerable variability in the threshold current and *f–I* slope values between cells. Therefore, for the rest of this study, when pooling data across cells, the equivalent input is expressed as the firing rate in the absence of oscillations. This was almost linearly related to the tonic current input in all cells, and provides a satisfactory normalization (Fig. 1*C*).

At low input levels, the presence of the theta oscillation primarily resulted in an elevation of firing rate relative to the oscillation-free case; at higher input levels both relative elevation and suppression of firing rate were apparent (Fig. 1*C*).

The phase of firing relative to the theta frequency oscillatory input was strongly dependent on the level of tonic excitation (Fig. 1*A* and *D–F*), as reported previously for hippocampal pyramidal cells (Kamondi *et al.* 1998) and mitral cells in the olfactory bulb (Margrie & Schaefer, 2003) *in vivo*. Recording *in vitro* affords precise control of electrical inputs to the cell (spontaneous synaptic inputs to CA1 pyramidal cells are minimal in the acute hippocampal slice), allowing us to investigate the details of this input-to-phase transform, which we will refer to as the phase–current (ϕ–*I*) curve.

Figure 1*D* shows spike phase histograms from a typical cell. At low, just suprathreshold levels of tonic input, spikes occurred at a phase of 55.4 ± 14.2 deg (taking phase zero to be the peak of the oscillatory current input). Examining the subthreshold membrane potential trace also shown in Fig. 1*D*, this phase range evidently lies close to the peak of the membrane potential oscillation (the phase shift between the theta frequency current input and voltage response for this cell was 44 deg). Above 1 spike per cycle, as the tonic excitatory drive to the cell increased, the phase of firing of the first spike in each cycle advanced monotonically, to -105.2 ± 20.2 deg at the highest levels of excitation tested (Fig. 1*D* and *E*).

Beyond a certain level of input, secondary and then tertiary spikes began to occur within each oscillatory cycle. These were similarly phase-locked and advanced with increasing tonic input, such that the interspike interval (ISI) between first and second spikes, and between second and third spikes was constant (91.2 ± 9.7 deg between first and second spikes, 93.7 ± 17.9 deg between second and third spikes).

As well as advancing the phase at which spikes occurred, the increasing excitation also allowed spikes to occur later in the cycle, so that at the point at which tertiary spikes began to arise, they occurred at 82.3 ± 23.0 deg, considerably later than the equivalent value for primary spikes (Fig. 1*D*). Note however, that the retreat of late spikes was not symmetrical with the advancement of early spikes (at the level of input discussed here, 30 deg of retreat compared to 160 deg of advance).

The pattern of behaviour described above for a typical cell was reflected consistently for the entire population of cells recorded ($n = 15$; Fig. 1*F*). Pooling data from all cells and levels of input, the mean standard deviation of spike phases at a fixed level of input was 17.5 ± 8.5 deg, corresponding to 9.7 ± 4.7 ms. Approximating the ϕ–*I* curve by a linear fit, the mean slope of theta phase advance (mean of individual cell phase advance slopes), expressed relative to the oscillation-free firing rate was -14.4 ± 5.7 deg Hz^{-1} (range -6.8 deg to -26.8 deg Hz^{-1}). That is, a change in tonic input which would, in the absence of oscillations, yield a 1 Hz increase in firing rate will yield an average advance of spike timing of 8.0 ms.

Gamma frequency input

We next assessed the relation between tonic input and firing in the presence of gamma frequency (40 Hz) sinusoidal input (Fig. 2).

The presence of the gamma oscillation did not change the slope of the *f–I* curve compared to the oscillation-free case (mean suprathreshold *f–I* regression slopes, 0.137 Hz pA^{-1} in the oscillation-free case;

0.144 Hz pA^{-1} with gamma oscillation included; paired *t* test $P > 0.1$, $n = 15$; Fig. 2*B*, *C*). No plateaux were observed for the input values tested.

With regard to the phase of firing, ϕ–*I* curves were strikingly different from those observed for theta frequency input. Cells did not entrain to the gamma oscillation, and the phase of firing was almost independent of tonic input level. The phase of firing was nonetheless restricted to only a portion of the oscillation cycle (Fig. 2*D*), with a mean phase across all levels of input of 55.8 ± 7.7 deg. The mean standard deviation of spike phase at a fixed level of input was 43.4 ± 4.9 deg. For this cell, phase of firing was statistically dependent on the level of tonic excitation (Fig. 2*E*; linear regression, $P < 0.05$) but with very low gradient (−1.672 deg Hz^{-1}), accounting for a very small proportion of the observed variance ($R^2 = 0.012$). Similar behaviour was observed across the population of cells recorded (Fig. 2*F*), with a mean phase of firing of 64.2 ± 16.1 deg, and a mean standard deviation around this of 47.1 ± 16.8 deg, corresponding

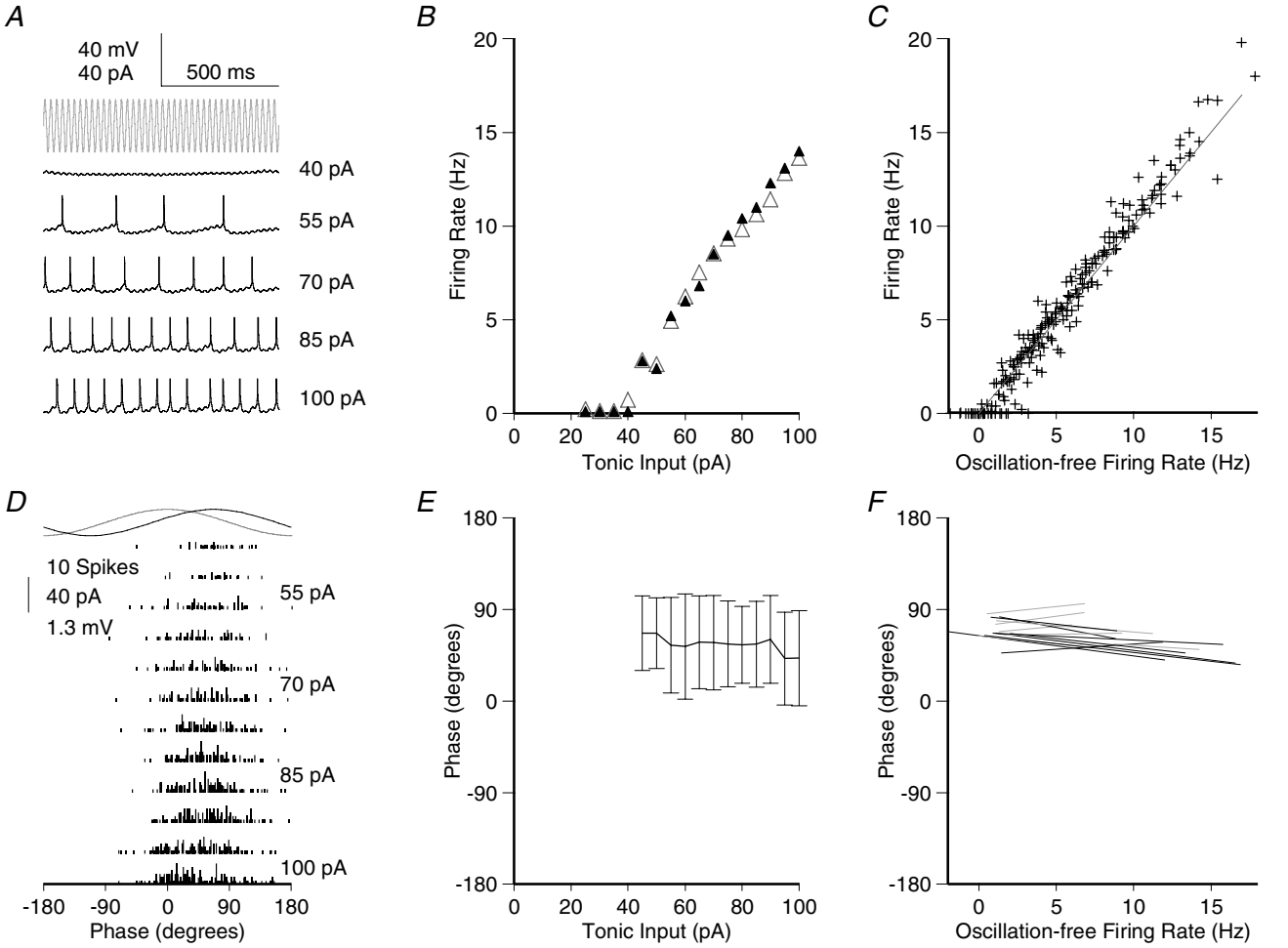

Figure 2. Phase of firing relative to gamma frequency sinusoidal current is minimally dependent on the level of tonic excitation for physiological firing rates
A, membrane potential traces for a typical cell (same as shown in Fig. 1*A*) receiving a fixed amplitude of gamma frequency (40 Hz) sinusoidal current input (trace indicated in grey at the top for comparison of timing) and a range of levels of tonic depolarizing current (indicated to the left of the traces). Spikes are truncated at –20 mV for clarity. *B, f–I* data for the same cell, with (filled symbols) and without (open symbols) sinusoidal gamma frequency current. The oscillatory component has strikingly little effect on the firing rate. *C, f–I* data for the population of cells recorded ($n = 15$), with input normalized across cells as described for Fig. 1*C*. *D,* spike time histograms for the same cell as in *A*, relative to the oscillatory cycle, across the range of tonic input levels tested. There was never more than one spike in any cycle. *E*, spike phase *versus* current curve for the same cell (mean ± S.D.). *F*, linear fits to phase *versus* oscillation-free firing rate curves for the population of cells. Cells with significant regression slope ($P < 0.05$) are shown in black, non-significant in grey. Mean slope of phase advance was 0.676 ± 1.51 deg Hz^{-1}, accounting for very little of the variance in spike phase (mean $R^2 = 0.015$). The mean standard deviation of firing phase was 47.1 ± 16.8 deg.

to 3.3 ± 1.2 ms. In 8 out of 15 cells, there was a significant dependence of phase on tonic input level (linear regression, $P < 0.05$). The slope of this was always very shallow, however, and while negative in most of those cells, it was in fact positive in 1 out of the 8. The mean slope of phase advance across all 15 cells was -0.68 ± 1.5 deg Hz^{-1}. This equates to a total phase advance of around 10 deg over the range of inputs tested, accounting for only a small proportion of the variance in the phase of firing (mean $R^2 = 0.015$).

Mathematical model of phase locking

We have demonstrated that the firing of hippocampal pyramidal cells receiving combined tonic excitation and oscillatory input will phase lock to the oscillation and systematically phase advance with increasing tonic input, if the oscillation is of low (theta, 5Hz) but not high (gamma, 40 Hz) frequency. Can the occurrence of these activity states be predicted and understood using a simple neuron model?

Following Gerstner & Kistler (2002), the membrane potential of a single-compartment leaky integrate-and-fire cell receiving both oscillatory and tonic current input, with voltage reset on reaching threshold, can be described as follows:

$$V_{\mathrm{m}}(t) = V_{\mathrm{R}} e^{-\frac{t-\hat{t}}{\tau_{\mathrm{m}}}} + I_{\mathrm{tonic}} R_{\mathrm{in}} \left(1 - e^{-\frac{t-\hat{t}}{\tau_{\mathrm{m}}}}\right) + I_{\mathrm{osc}} R_{\mathrm{in}} A \left(\cos(\omega t + \varphi) - e^{-\frac{t-\hat{t}}{\tau_{\mathrm{m}}}} \cos(\omega t + \varphi)\right) \quad (1)$$

where $V_{\mathrm{m}}(t)$ is the membrane potential at time t, V_{R} the reset potential following the most recent spike at time $\hat{t}$, τ_{m} the membrane time constant, R_{in} the input resistance, ω equal to $2\pi f$ radians, I_{tonic} the tonic current input, I_{osc} the amplitude of the oscillatory current sinusoid, and

$$A = \frac{1}{\sqrt{1 + (\omega\tau_{\mathrm{m}})^2}} \quad (2)$$

$$\varphi = -\arctan(\omega\tau_{\mathrm{m}}) \quad (3)$$

Note that these equations treat the resting membrane potential as 0 mV.

Phase locking can be approached analytically by solving for t under the condition that the membrane potential reaches threshold at a time after the preceding spike equal to the period (p) of the oscillation, i.e. set $V_{\mathrm{m}}(t) = V_{\mathrm{th}}$ and $t - \hat{t} = p$. The spike phase, ϕ, is then:

$$\phi = \arccos\left(\frac{V_{\mathrm{th}} - V_{\mathrm{R}} e^{-\frac{p}{\tau_{\mathrm{m}}}}}{\left(1 - e^{-\frac{p}{\tau_{\mathrm{m}}}}\right) I_{\mathrm{osc}} R_{\mathrm{in}} A} - \frac{I_{\mathrm{tonic}}}{I_{\mathrm{osc}} A}\right) - \varphi \quad (4)$$

Equation (4) has two real solutions (within the range for which real solutions exist at all, that is when the terms within the arccos brackets fall in the range -1 to 1), one on the up-slope and one on the down-slope of the sinusoidal component. Naturally, only the former is valid in the current context of membrane potential rising to threshold.

The model predicts that, as I_{tonic} increases, cells will enter a phase locked firing regime, with one spike per oscillation cycle, initially at the peak of the membrane potential oscillation. Further increases in I_{tonic} will yield an advance of the firing phase, exactly as we recorded for the first spike per cycle in cells receiving theta frequency oscillatory input. As shown by Fig. 3, the arccos function suggested by the above equations provides a satisfactory fit to the ϕ–I curves obtained experimentally. Figure 3 shows the predicted ϕ–I curve for a cell with basic membrane properties matching the mean of our experimentally recorded cells ($R_{\mathrm{in}} = 144$ MΩ; $\tau_{\mathrm{m}} = 24$ ms), along with ϕ–I curves from three example cells, fit by arccos functions. Note that the experimentally recorded ϕ–I curves presented are substantially broader than predicted analytically, even allowing for a fall in R_{in} and τ_{m} when depolarized and spiking. In the limit as τ_{m} approaches zero, A approaches 1, and the ϕ–I curve approaches its maximum width of $2I_{\mathrm{osc}}$, or in the case of our experiments, 80 pA. Active properties of the neurons in question can account for this discrepancy, notably resonance in the theta frequency range (Pike *et al.* 2000; Hu *et al.* 2002) and attenuation of the response to tonic current, due to I_{h}. Apart from this scaling factor, the arccos function provides a very satisfactory fit to the experimental data.

Using the equations derived above, it is straightforward to predict the system behaviour for changes in oscillation parameters (amplitude or frequency) or intrinsic cell properties (R_{in} and τ_{m}), as Fig. 4 makes explicit. Of note is the robustness of the ϕ–I curve shape to changes in the conductance state of the cell: for a fourfold reduction in τ_{m}, the slope of the ϕ–I curve decreases by only 1.167. These figures refer specifically to the parameters presented in Fig. 4*E* (for a 5 Hz oscillation, and a shift in τ_{m} from 20 ms to 5 ms). This relationship becomes substantially steeper as τ_{m} or oscillation frequency increases: for example, for a 40 Hz oscillation, the same shift in τ_{m} would yield a decrease in ϕ–I curve slope of 2.29. This can be understood by examining the value of A (eqn (2)) as a function of τ_{m} and oscillation frequency.

Outside of the critical range of I_{tonic} which yields phase locked states, the cell will either be entirely subthreshold, or else enter less regular firing regimes (see Tiesinga *et al.* 2002; Brody & Hopfield, 2003). As our recordings for gamma frequency input illustrate, the phase of firing can still be restricted in this case, because the membrane potential trajectory is only positive for a fraction of the

oscillation cycle (see Fig. 5), but no strong, systematic dependence of phase on tonic input level is established. As is apparent in Fig. 5*C*, some advance of spike phase with increasing I_{tonic} could be expected, but the extent of this is slight when compared with the variance in spike phase due to other factors.

The system described by the above equations corresponds to the first plateau in the *f–I* curve we recorded for theta frequency input, since it describes an oscillation-locked firing state with one spike per cycle. Note that the equation is entirely insensitive to multiple threshold crossings within a single cycle, so that this analytical description of phase locking is no longer valid as firing rate increases beyond the first plateau. However, as outlined below, for some sets of parameters the phase of the first spike per cycle may be analytically predictable regardless of the presence of multiple spikes per oscillatory cycle.

Pseudo phase-locking

An important extension to the above account is suggested by our recordings from cells receiving theta frequency input. In that case, it is clear that secondary and higher order spikes per cycle can arise *without* disrupting the smooth phase advance of the first spike per cycle (although, for a few cells, a very slight non-linearity in the ϕ–*I* curve is apparent at the point at which secondary or tertiary spikes arise).

Consider the case in which the cell membrane time constant, τ_m, is substantially less than the oscillation period. From one cycle to the next, all of the exponentially decaying terms in the above equations approach zero. As a result, phase locking is not restricted to the firing rate plateaux. This will hold true for any set of parameters for which the sum of tonic and oscillatory currents is subthreshold for sufficient duration to allow system reset (adequate decay of the exponential terms).

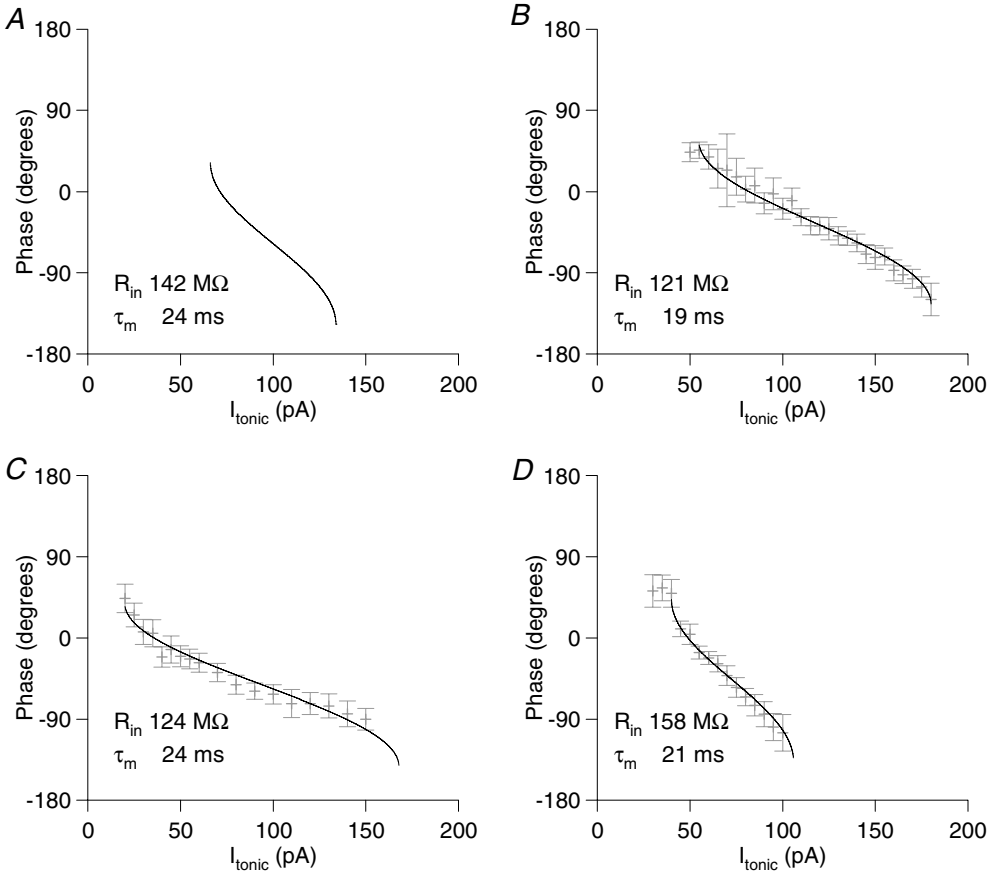

Figure 3. Analytically predicted and experimentally measured ϕ–*I* curves
A, the analytically predicted ϕ–*I* curve for a passive point neuron model with basic membrane properties matching the mean of our recorded cells ($R_{\text{in}} = 142$ MΩ, $\tau_m = 24$ ms). *B–D*, ϕ–*I* curves from typical cells, fit by an arccos function, as suggested by the analytical model (phase extent of ϕ–*I* curve fits fixed at 180 deg in keeping with the model, but phase lag and slope of the curve allowed to vary freely). The R_{in} and τ_m values reported for each cell were recorded at resting membrane potential. Note that ϕ–*I* curves for the experimentally recorded cells are frequently wider than can be accounted for in the passive model (the upper limit on ϕ–*I* curve width, as τ_m approaches zero is twice the oscillatory current amplitude, or 80 pA in this case; see text for discussion).

Extension from tonic to phasic currents

We can easily extend this description of the system to include intermittent excitation. Assuming again that the membrane time constant is sufficiently shorter than the oscillation period, it is possible to significantly alter the fraction of the cycle for which a given level of step current is active without substantially changing the phase of firing (assuming that the step is applied in the period leading up to the time of firing). Equivalently, only modest increases in excitatory current step amplitude are required to compensate for substantial reductions in step duration (Fig. 6).

It is relatively simple to go further to an intuitive understanding of how the system will respond to changes in the temporal structure of the input, with the proviso that active properties of the cell may significantly confound this intuition.

Current *versus* conductances

Oscillations in real neurons arise not as a result of applied current, but of conductance changes. How does this change the behaviour of the system, compared to that described above?

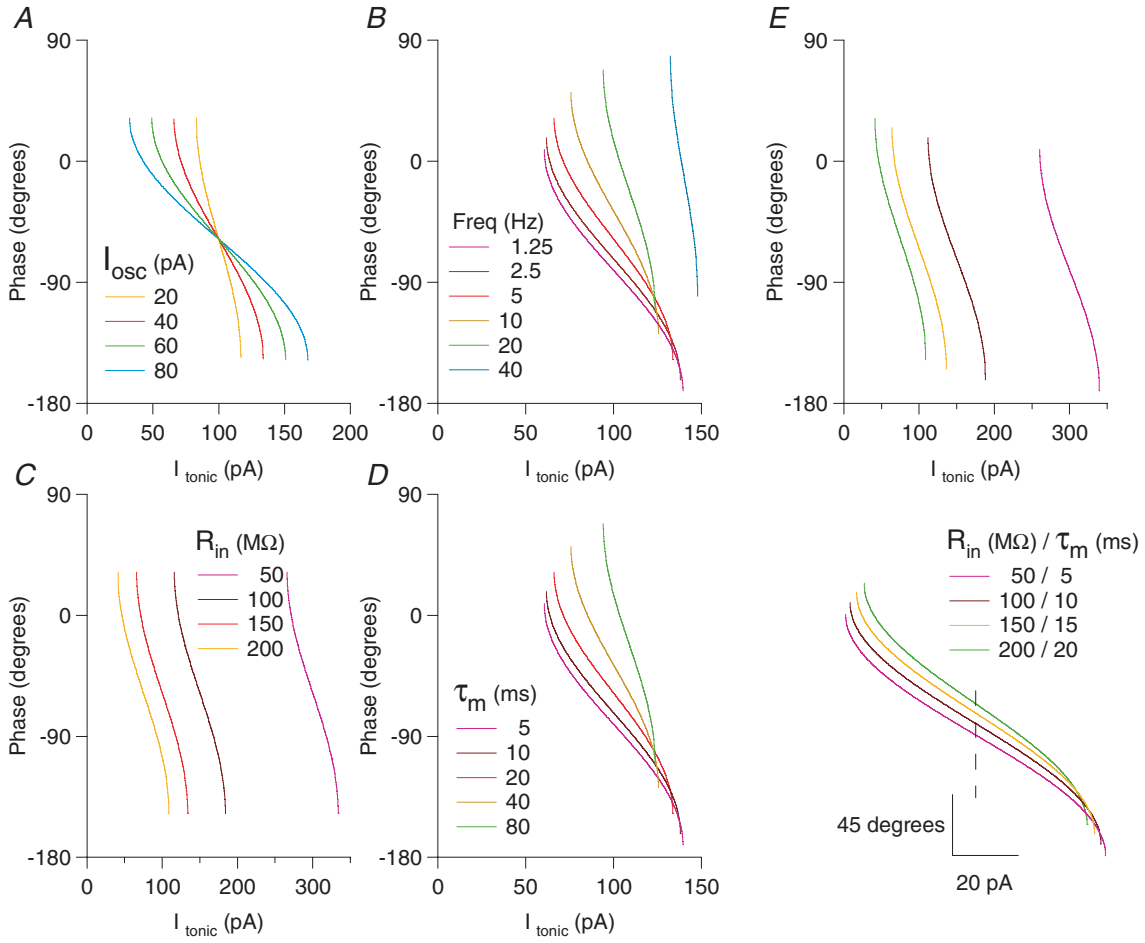

Figure 4. Analytically predicted ϕ–I curves for variations in oscillation parameters (amplitude and frequency) and intrinsic cell properties (R_{in} and τ_m)
Analytically derived ϕ–I curves for a passive point neuron model with the following parameters, except where otherwise stated: $R_{in} = 150$ MΩ, $\tau_m = 20$ ms, $I_{osc} = 40$ pA, oscillation frequency $= 5$ Hz (these default values shown by the red traces). *A*, increasing oscillation amplitude leads to horizontal stretch of the *f*–*I* curve, symmetrical about its midpoint. *B*, increasing oscillation frequency leads to an upward and rightward shift of the ϕ–I curve, along with an increase in its slope. *C*, decreasing R_{in} leads to a rightward shift of the ϕ–I curve, with no effect on curve slope or phase lag. *D*, changing τ_m has an effect identical to proportional changes in oscillation frequency. *E*, parallel changes in R_{in} and τ_m (as seen with, e.g. a change in net synaptic drive to a cell) yield a simple combination of the effects of independent changes in R_{in} and τ_m. Specifically, increased τ_m and R_{in} yields a left shift of the curve, with increased phase lag and an increase in slope. In the lower panel of *E*, ϕ–I curves have been horizontally aligned by the midpoint (dashed line), emphasizing that substantial changes in conductance state of the cell could yield surprisingly small changes in the shape of ϕ–I curve (dependent on specific parameters; see text for details).

In the CA1 region of the hippocampus, at least part of the theta oscillation in pyramidal cells is thought to arise from rhythmically modulated perisomatic inhibitory conductance inputs, driving a chloride conductance, with a reversal potential therefore only ~20 mV negative to the working range of the cell.

In order to test for any specific effects of oscillatory conductance (as opposed to current) input, we simulated inhibitory theta input in pyramidal cells *in vitro* using dynamic clamp ($n = 14$). Excitatory inputs to these cells are mostly electrotonically fairly distal, and so we implemented the depolarizing drive as a current rather than a conductance, bearing in mind the relatively short conductance length constant reported for pyramidal neurons (Williams, 2004).

From Fig. 7*A* it is clear that neuronal behaviour during conductance-based oscillatory input is not fundamentally different from that during current-based input. Figure 7*B* compares the population responses in the current and conductance cases (normalized by the firing rate to a given level of tonic input alone, in the absence of oscillatory input). The extent and slope of the phase curves are very similar in the two cases (the horizontal offset of the ϕ–I curves is because the oscillatory component in the current-based case contributes zero mean current, whereas in the conductance-based case the oscillation introduces a mean inhibition). We might expect that, for conductance-based oscillations, increasing depolarization at high levels of tonic current input would lead to a larger amplitude oscillation, decreasing the slope of the ϕ–I curve. There is some indication that this occurs, but even so, the effect is small, and restricted to the highest input levels tested. Thus, this simple, analytical model holds well also for conductance-based oscillations.

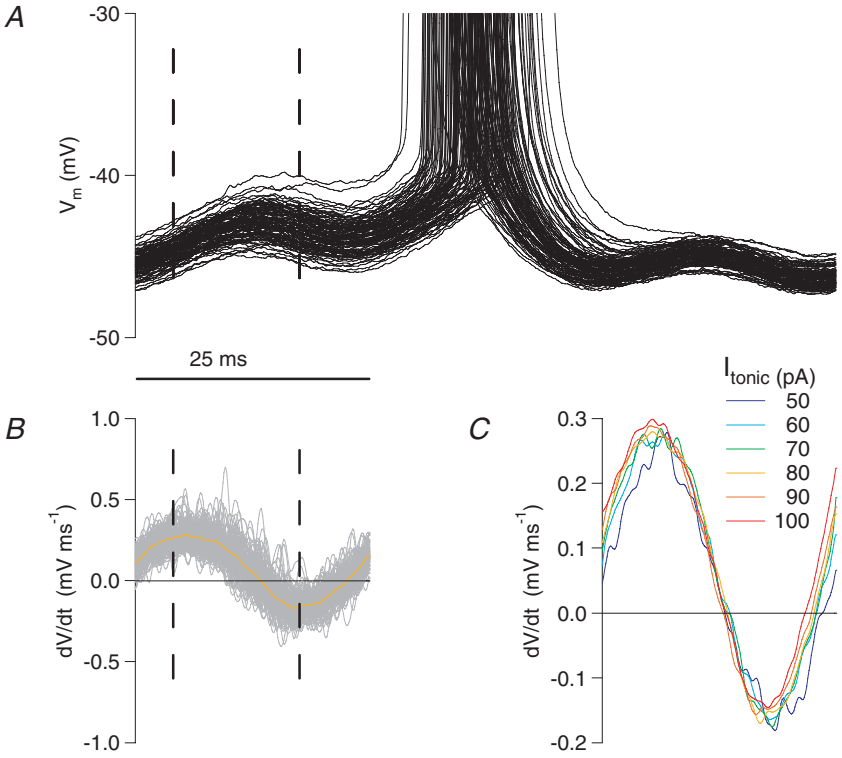

Figure 5. Peri-threshold membrane potential behaviour during gamma frequency input
A, peri-spike membrane potential traces for a cell receiving a fixed level of tonic input (80 pA) and fixed amplitude sinusoidal oscillatory input at gamma frequency (40 pA, 40 Hz), aligned by oscillation phase. Dashed lines in the cycle preceding the spikes indicate the phase range over which spikes occurred. Note that, in the cycle preceding the spike, there is always a downwards trend in membrane potential late in the cycle. The implication is that, if the cell has not spiked by a certain point in the cycle, the trough of the oscillatory input is sufficient to overcome the cell's intrinsic inward currents and postpone spiking to the next gamma cycle. *B*, the first derivative of the above traces (mean shown in orange) emphasizes the negative slope of the membrane potential for part of the cycle preceding spiking. *C*, mean of membrane potential first derivatives (as in *B*) for different levels of tonic input. With regard to the phase at which positive membrane potential slope resumes late in the cycle, note that this advances systematically with increasing tonic input. As reflected in the ϕ–I curves for gamma frequency input, however, this advance is slight compared with the overall variance in spike phase.

Encoding efficiency of firing rate and phase

How efficiently do the rate and phase of firing convey information about the tonic input to a cell during oscillations?

One way to approach this question is to estimate the mutual information between the tonic current input level and either the rate or the phase of firing (Shannon, 1948; Borst & Theunissen, 1999). In doing so, we are confronted with a choice of methods. We could estimate the mutual information from the recorded data directly, and incorporate a measure to compensate for the bias introduced by discrete sampling of the stimulus range (e.g. Panzeri *et al.* 2007). Alternatively, we can describe response probabilities as a continuous function of the input, deriving the relevant parameters from the data, and estimate mutual information on that basis. Since we have a theoretical basis for the form of this function, which yields a good description of the data, we opt for the latter approach (see Methods).

Up to this point we have considered transforms of input to rate or phase. The phase transform is, of course, only valid in the presence of oscillatory activity. In comparing the mutual information content of the different transforms, it is interesting to ask whether any differences are due to the presence of the oscillatory activity itself, or whether they depend on fundamental differences in the nature of spike count (discrete variable) and spike timing (continuous variable) coding schemes. Does an equivalent to the phase transform exist in the non-oscillatory regime? In the absence of an external temporal reference against which to judge the timing of spikes, any temporal reference must be intrinsic to the neuron itself. Thus, the equivalent transform is the interspike interval (ISI).

Figure 8*A* shows the mutual information estimates for the population of cells recorded with theta oscillatory input implemented as an inhibitory conductance using dynamic clamp ($n = 14$), assessed for a range of windows of temporal integration (0.2–1.0 s, or equivalently 1–5 theta cycles). The temporal codes (phase and ISI) were more efficient than the rate codes. Figure 8*B* shows the mean and standard deviation of within-cell information differences for the various codes.

Comparing the phase and rate codes, the phase code yields significantly more information over all relevant time intervals (paired t tests, $P < 0.001$ for phase code *versus* rate codes both with and without oscillations). Comparing the phase code to the rate code in the absence of oscillations, after 0.2 s, the mean difference in information ($\pm$ S.D.) was 1.27 ± 0.37 bits (mean of differences for individual cells); and after 1 s, 1.07 ± 0.47 bits. Comparing the phase code to the rate code with oscillations, the difference in information was 1.12 ± 0.31 bits after 0.2 s, and 1.35 ± 0.38 bits after 1 s.

In order to transmit the same information available in one theta cycle via the phase code, the rate code had to be evaluated over nearly 0.85 s, or a 4.25 times greater interval. Equivalently, more than four neurons encoding

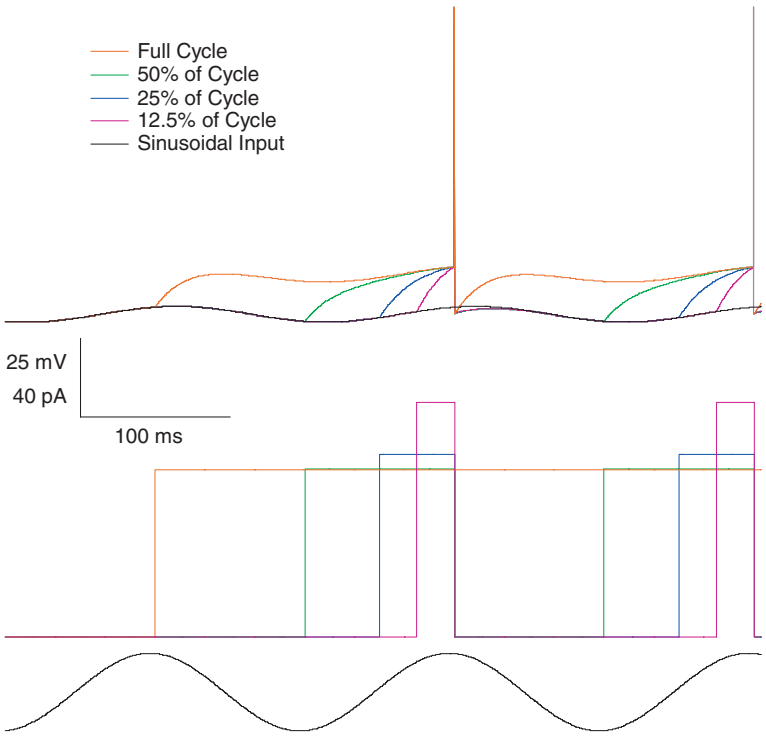

Figure 6. Excitatory current step duration and amplitude trade-off for fixed spike phase
Output from a numerically simulated single compartment integrate-and-fire model (lower traces show the tonic and oscillatory current inputs, upper traces show the resulting membrane potential). With shortening of the excitatory current step duration, spike phase can be maintained by modest increases in step amplitude. For the physiologically relevant parameters tested here (5 Hz oscillation, τ_m 20 ms), reducing step duration to only 50% of the oscillation cycle necessitates only a 0.67% increase in step amplitude, and even for a step duration of 12.5% of the cycle, a 40% increase in step amplitude compensates.

the same information would be required using a rate code to match one neuron using a phase code. Naturally, each neuron need not encode the same information, but even in the limit of allowing each neuron to encode independent information, the phase code would be more than twice as efficient over a single theta cycle.

The performance of the ISI code was very similar to that of the phase code, with a mean difference in information of 0.15 ± 0.46 bits after 0.2 s; and 0.17 ± 0.51 bits after 1.0 s (difference not statistically significant).

Comparison of the rate codes in the presence and absence of oscillatory input is also of interest. The rate code in the presence of oscillations was marginally superior to the oscillation free rate code at short estimation intervals (0.12 ± 0.16 bits at 0.2 s; paired t test $P < 0.05$), but was superseded as the estimation interval increased (-0.33 ± 0.22 bits at 1.0 s, paired t test $P < 0.005$). This reflects the tendency towards cycle locking of spikes, which reduces the uncertainty in the response to a given level of input, thereby increasing the information available over short intervals. However, over longer intervals, the cycle locking reduces the number of different response states available to the cell (or at least skews the distribution of responses towards a minority of the possible states), reducing the total response entropy and thus decreasing the mutual information.

Discussion

Basic principles of the rate-to-phase transform

We have set out a basic framework for the understanding of a neuronal rate-to-phase transform, and the circumstances under which it will arise.

According to this framework, any neuron receiving tonic excitatory drive combined with slow oscillatory input (oscillation period long compared to τ_m) will implement a rate-to-phase transform, with an increase in tonic drive yielding advance of the first spike per cycle. Our *in vitro* recordings demonstrated that real neurons (in this case, hippocampal CA1 pyramidal cells) will readily implement this transform given appropriate oscillation

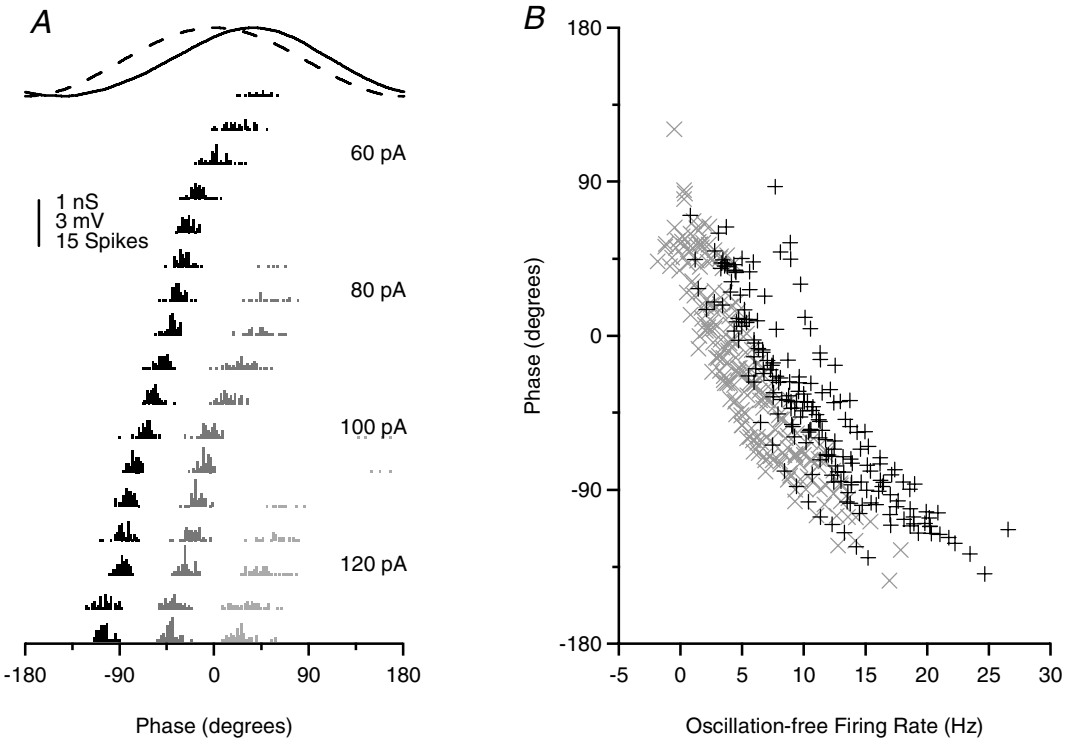

Figure 7. Cell response to oscillatory conductance injection, via dynamic clamp, does not differ significantly from oscillatory current injection

A, spike phase histograms for a typical cell receiving a theta frequency (5 Hz) sinusoidally modulated inhibitory conductance (implemented via dynamic clamp) and a range of levels of tonic current input. First spike per cycle are indicated in black, second in dark grey, and third in light grey. The conductance input (dashed line) and subthreshold membrane potential response (continuous line) are also indicated. Note that, because it is inhibitory, the conductance trace is inverted for clarity of presentation. *B*, comparison of ϕ–I scatter plots for current based (grey) and conductance based (black) oscillatory input. Apart from a horizontal shift due to the mean inhibitory component of the oscillatory conductance, no qualitative difference in behaviour is revealed.

parameters (here, 5 Hz oscillatory input of physiologically relevant amplitude). In the context of temporal coding schemes, this transform resembles latency-to-first-spike codes which have now been identified for a number of systems (Johansson & Birznieks, 2004; Gollisch & Meister, 2008), with two additional features. First, latency has typically been measured relative to some external reference, such as stimulus onset, whereas for the oscillatory rate-to-phase transform, the oscillation itself serves as temporal reference. Second, the oscillation based code has the further advantage that it will be repeated or updated on each cycle.

The computational power of such an oscillation-based coding system has been previously described, using a theoretical model (Hopfield, 1995). This was further supported by a subsequent study, demonstrating that the neuronal behaviour required by that model could be implemented by mitral cells of the mouse olfactory bulb *in vivo* (Margrie & Schaefer, 2003).

The oscillatory rate-to-phase transform described could also underlie codes based on the order of first spikes across cells (Thorpe *et al.* 2001) rather than on spike phase *per se*.

Gamma frequency oscillations

Our experiment did not uncover a rate-to-phase transform in CA1 pyramidal neurons using purely tonic input on a gamma frequency (40 Hz) oscillation, at least in part because they could not sustain a sufficiently high

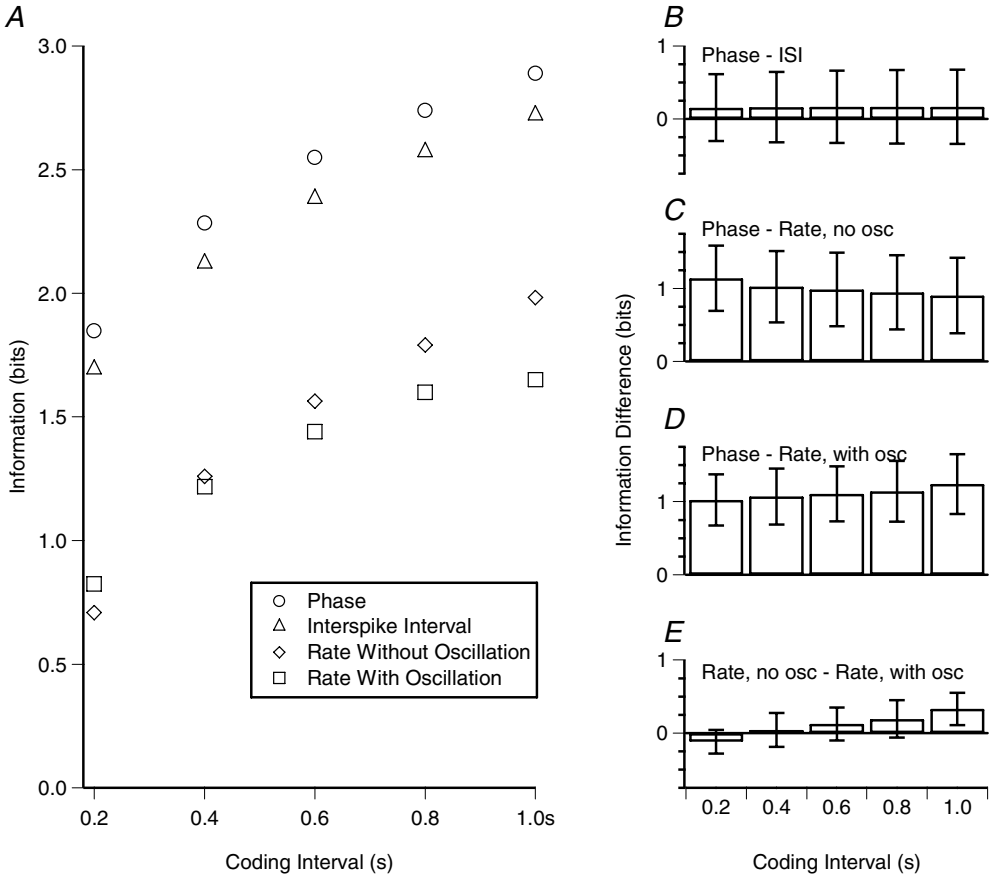

Figure 8. For CA1 pyramidal cells encoding tonic input level, temporal codes are more information efficient than rate codes

A, mean mutual information across cells (those tested in dynamic clamp mode, $n = 14$), between I_{tonic} and each of the spike output parameters (phase, ISI or rate), as a function of the coding interval (time period for examination of the spike output). Error bars are not indicated because a major source of variance across cells was the stimulus range over which information was estimated. *B–E*, differences in information estimated for each of the spike output parameters (mean and standard deviation of individual cell differences). Information *difference* values are not sensitive to the stimulus range over which they are estimated (given equally efficient coding across all relevant stimulus levels, which we found to be nearly the case), and so error bars are included for panels *B–E*. Temporal codes (phase and ISI) were not significantly different from each other ($P > 0.05$) but were both significantly more efficient than rate codes ($P < 0.001$).

firing rate. However, this is unlikely to be a general limitation for phase coding. Indeed, several classes of neuron exhibit faster τ_m and can fire at higher rates than hippocampal pyramidal cells, and thus, according to our model, would be likely to implement a rate-to-phase transform at higher oscillation frequencies. Even hippocampal pyramidal cells might be able to support gamma phase coding *in vivo*. First, during gamma activity *in vivo*, pyramidal neurons are likely to have faster τ_m than we observe *in vitro*. Secondly, although these neurons are unable to sustain high frequency firing to tonic input, fluctuating inputs as seen *in vivo* may allow the spike phase to be controlled relative to the gamma oscillation over brief time intervals.

Tiesinga *et al.* (2002) studied entrainment of *interneuron* firing to gamma frequency oscillatory input, and the associated mutual information between input level (actually, in their case, the number of inhibitory inputs per cycle, but this is in effect equivalent to the level of tonic input we describe) and output spike phase. As might be expected given the faster τ_m of these cells and their intrinsic potential to sustain higher firing rates, a phenomenon closely resembling the rate-to-phase transform was observed, but specifically in the entrained state, that is, where there was strictly one spike per cycle. This conforms to the system described by eqn (4) and would be equivalent to observing control of firing phase only on the firing rate plateaux (for theta frequency input in our case; Fig. 1*B*). This version of the rate-to-phase transform is the basis of several recent models (Brody & Hopfield, 2003; Hopfield, 2004; Hopfield & Brody, 2004).

We wish to emphasize an important functional difference between this entrainment-specific rate-to-phase transform and the theta frequency rate-to-phase transform that we report, where phase locking is not restricted to the oscillation-entrained firing state. This difference is dependent on the oscillation period being sufficiently longer than the neuronal τ_m, and yields an important difference in the context of information coding. For fast oscillatory input, a substantial proportion of the possible input levels may result in non-phase-locked firing across a substantial fraction of the oscillation cycle (apparent in Tiesinga *et al.* 2002; Brody & Hopfield, 2003; Hopfield, 2004; Hopfield & Brody, 2004). This is true for input levels both higher and lower than the range yielding entrained firing, so that the phase of firing might not be unambiguous for downstream neurons, which, for efficient use of this code, would also need to be informed whether or not the signalling neuron was operating in the entrained range. For slow oscillatory input, such as we demonstrate for theta frequency input, this signal ambiguity is avoided. If the cell fires at all, the rate-to-phase transform is implemented, at least up to levels of input yielding maximal phase advance (180 deg relative to threshold phase).

Note also that, in the fast oscillation regime, spike timing in one cycle is dependent on the timing of the spike in the previous cycle. This has two significant consequences. Firstly, when there is a change in tonic input to the cell, phase of firing may not shift immediately to the analytically predicted value, but rather iterate towards it over the course of several cycles. Secondly, transient events which perturb the spike phase in a given cycle would have effects on spike timing in subsequent cycles. This is not true of the slow oscillation regime, in which spike phase will match analytical predictions within the cycle following a change in tonic input level, and within the same cycle if the input change occurs early relative to the analytically predicted spike time. Similarly, the subthreshold period of the oscillation allows spike timing in each cycle to be independent of events in the preceding cycle. Of course, active neuronal properties with sufficiently slow dynamics may influence subsequent cycles, as has been described in the context of phase response curves (Lengyel *et al.* 2005).

Hippocampal phase precession and the rate-to-phase transform

The phenomenon of phase precession in hippocampal place cells provides the best evidence of a phase code in the mammalian CNS (O'Keefe & Recce, 1993). What are the implications of our results for the understanding of place cell phase precession?

The results presented here suggest that, for phase coding, the phase of only the first spike per cycle should be used to infer information about the input, rather than the phase of all spikes or the mean phase.

The neuron-level processes underlying the generation of place cell phase precession have not yet been identified. Putative mechanisms include a transform of excitation to phase (Harris *et al.* 2002; Mehta *et al.* 2002), much as we describe here, or the interference between two or more oscillations (O'Keefe & Recce, 1993; Kamondi *et al.* 1998; Magee, 2001; Lengyel *et al.* 2003; Burgess *et al.* 2007). It is worth noting that place cells *in vivo* are reported to advance monotonically through a full 360 deg as the place field is traversed. Our results demonstrate that the simple combination of varying tonic input on fixed oscillations can only account for controlled phase advance over at most 180 deg (non-sinusoidal rhythmic input patterns could increase the useable fraction of the cycle, but the requirement for a subthreshold period would remain). Higher levels of tonic input would yield non-phase-locked firing, unrestricted by oscillation phase.

We note, however, that place cell phase precession is not uniform across the place field. Plots of place cell phase data presented in the literature exhibit two distinct trends (O'Keefe & Recce, 1993; Harris *et al.* 2002; Mehta *et al.* 2002; Huxter *et al.* 2003). This observation has received

quantitative support (Yamaguchi *et al.* 2002). On entry to the place field, phase of firing is well restricted and advances smoothly over the first 180 deg of the oscillation cycle, in a manner strikingly consistent with that predicted by the rate-to-phase transform which we describe. In the latter part of the place field, phase of firing is less well restricted, occupying the remaining 180 deg of the oscillation cycle. This cannot be accounted for by a simple rate-to-phase transform as presented here. However, it would be consistent with firing in the less ordered regime entered when cells are driven beyond 180 deg of phase advance, provided there were some mechanism to inhibit firing around the oscillation peak.

Kamondi *et al.* (1998) recorded from rat hippocampal pyramidal cells *in vivo*, with a specific interest in the phenomenon of place cell phase precession. They demonstrated the potential for cells to implement the rate-to-phase transform that we describe, with the same limitation of 180 deg of phase advance. Likewise, they qualitatively report asymmetry of spikes around the oscillation peak (most spikes on the upslope), similar to what we found. In a model, they were able to reproduce this behaviour by the introduction of a slowly activating outward current (specifically I_{KS}, although one can envisage that, in general, a similar effect will be generated by any adapting currents, be they spike activated or slow voltage dependent). Our analytical results highlight an important role for this type of mechanism. By extending the effective subthreshold period of the oscillation, the system has more time to 'reset', so that the late spikes from one cycle do not interfere with the timing of the first spike in the next. Indeed, without such a mechanism, even 180 deg of well controlled phase advance would not be possible. We note that, from the results presented by Margrie & Schaefer (2003), considerably less asymmetry of firing is present in mitral cells of the mouse olfactory bulb (approximately 80 deg advance for 55 deg retreat, measured from their figures, compared to, e.g. 160 deg advance for 30 deg retreat in our data). Whatever the reasons for these differences, their presence hints at a functional relevance.

Efficiency of coding

Consider a system which must convey information about some input signal that it receives. The rate with which it can transmit information is limited by the number of distinct responses it can generate within a given interval (with each response representing the presence of a different input). Shannon (1948) set out a mathematical framework to quantify this. For neurons implementing a rate code, this value is set by the range of firing rates, a discrete number. In the context of a temporal code, however, the output variable is continuous – if times of firing could be determined precisely as real numbers, then the system would have the potential to transmit infinite information per signal. Of course, in reality this is limited by noise and the potential of the neuronal hardware to generate (and for the receiving neurons, to distinguish) precisely timed spikes.

Efforts to derive information capacity limits for single neurons using rate or temporal codes began soon after Shannon developed his information theory framework (Mackay & McCulloch, 1952; Rapoport & Horvarth, 1960; Stein, 1967), but have been hampered by the paucity of relevant physiological data. More recent studies have tended to examine the efficiency with which neurons in sensory systems can encode external stimuli (Rieke *et al.* 1997) but are limited in what they can tell us about the transforms performed by individual neurons, or their efficiency in doing so.

Other recent studies have characterized the temporal precision with which neurons can generate spikes (Mainen & Sejnowski, 1995; Schaefer *et al.* 2006). Indeed, Schaefer *et al.* (2006) examined specifically the role of oscillations in enhancing this precision. While they did not explore these effects in terms of the information content, it is clear that some of the phenomena that they describe (the role of the subthreshold period imposed by the oscillation, and the improved spike discrimination during the oscillation trough and upstroke) are consistent with the theta frequency phase transform which we have explored here.

The data we recorded offered the possibility to estimate directly the information available in the rate or timing of firing of a single neuron, for a simple input signal, and explicit, well characterised transforms. We found that, for the system studied, significantly more information was available via the temporal codes (phase or ISI) than via the rate code. This additional information could account for the increase in accuracy of position reconstruction from place cell activity when phase information was included (Jensen & Lisman, 2000).

It is striking that the phase code is as efficient as the ISI code – no information is lost by the addition of an external oscillation. At the same time, this oscillation provides a common temporal reference, enabling a code based on the rank order of spikes across a population of cells which could be read out by a simple biophysical mechanism (Gautrais & Thorpe, 1998; Thorpe & Gautrais, 1998), as well as facilitating the computations that can be performed using phase as stimulus representation (Hopfield, 1995). We are not aware of a physiologically based mechanism which could efficiently read out an ISI code.

The higher coding efficiency afforded by phase coding might also be important given the spatial constraints on neuron numbers (both in terms of physical space occupied and wiring distances). Depending on the way information is distributed across different neurons, rate coding would require from two to five times as many cells

to match the information transmission of the phase code (for the parameter set we explored; presumably for other parameter values and cell types, the relative efficiency of rate and phase coding systems would be different).

Multiple factors will influence the efficiency of information transfer in the phase coding regime. Notably, we tested cell responses with purely tonic input, whereas physiological inputs to the cell are composed of multiple discrete synaptic events. It is to be expected that this input noise will affect rate and phase codes to different extents. Furthermore, the influence of noise on phase coding will vary with oscillation parameters, such as amplitude and frequency. In this context, however, we note that Schaefer and colleagues found similar enhancement of spike precision *in vivo*, and for simulated oscillations *in vitro* (Schaefer *et al.* 2006), so that for some systems at least, the high information content which we estimate for phase coding is likely to be valid *in vivo*. The question of optimal performance in the phase coding regime is further complicated by the fact that the rate of signal update is linked to the coding mechanism: slow oscillations will typically allow more accurate signal discrimination, but at the expense of a lower rate of signal update. Thus, rapidly changing parameters may require faster oscillations for optimal encoding. We would suggest that this variability in the requirements of specific systems may in part account for the range of different oscillatory states encountered in the mammalian brain.

References

Adrian E (1926). The impulses produced by sensory nerve endings: Part I. *J Physiol* **61**, 49–72.

Borst A & Theunissen FE (1999). Information theory and neural coding. *Nat Neurosci* **2**, 947–957.

Brody CD & Hopfield JJ (2003). Simple networks for spike-timing-based computation, with application to olfactory processing. *Neuron* **37**, 843–852.

Bryant HL & Segundo JP (1976). Spike initiation by transmembrane current – white-noise analysis. *J Physiol* **260**, 279–314.

Burgess N, Barry C & O'Keefe J (2007). An oscillatory interference model of grid cell firing. *Hippocampus* **17**, 801–812.

Gautrais J & Thorpe S (1998). Rate coding versus temporal order coding: a theoretical approach. *Biosystems* **48**, 57–65.

Gerstner W & Kistler W (2002). *Spiking Neuron Models*. Cambridge University Press, Cambridge.

Gollisch T & Meister M (2008). Rapid neural coding in the retina with relative spike latencies. *Science* **319**, 1108–1111.

Harris KD, Henze DA, Hirase H, Leinekugel X, Dragoi G, Czurkó A & Buzsáki G (2002). Spike train dynamics predicts theta-related phase precession in hippocampal pyramidal cells. *Nature* **417**, 738–741.

Hopfield J (1995). Pattern recognition computation using action potential timing for stimulus representation. *Nature* **376**, 33–36.

Hopfield JJ (2004). Encoding for computation: Recognizing brief dynamical patterns by exploiting effects of weak rhythms on action-potential timing. *Proc Natl Acad Sci U S A* **101**, 6255–6260.

Hopfield JJ & Brody CD (2004). Learning rules and network repair in spike-timing-based computation networks. *Proc Natl Acad Sci U S A* **101**, 337–342.

Hu H, Vervaeke K & Storm JF (2002). Two forms of electrical resonance at theta frequencies, generated by M-current, h-current and persistent Na^+ current in rat hippocampal pyramidal cells. *J Physiol* **545**, 783–805.

Huxter J, Burgess N & O'Keefe J (2003). Independent rate and temporal coding in hippocampal pyramidal cells. *Nature* **425**, 828–832.

Jensen O & Lisman JE (2000). Position reconstruction from an ensemble of hippocampal place cells: Contribution of theta phase coding. *J Neurophysiol* **83**, 2602–2609.

Johansson RS & Birznieks I (2004). First spikes in ensembles of human tactile afferents code complex spatial fingertip events. *Nat Neurosci* **7**, 170–177.

Kamondi A, Acsády L, Wang XJ & Buzsáki G (1998). Theta oscillations in somata and dendrites of hippocampal pyramidal cells in vivo: Activity-dependent phase-precession of action potentials. *Hippocampus* **8**, 244–261.

Lanthorn T, Storm J & Andersen P (1984). Current-to-frequency transduction in CA1 hippocampal pyramidal cells – slow prepotentials dominate the primary range firing. *Exp Brain Res* **53**, 431–443.

Lengyel M, Kwag J, Paulsen O & Dayan P (2005). Matching storage and recall: hippocampal spike timing-dependent plasticity and phase response curves. *Nat Neurosci* **8**, 1677–1683.

Lengyel M, Szatmáry Z & Érdi P (2003). Dynamically detuned oscillations account for the coupled rate and temporal code of place cell firing. *Hippocampus* **13**, 700–714.

Mackay DM & McCulloch WS (1952). The limiting information capacity of a neuronal link. *Bull Math Biophys* **14**, 127–135.

Magee JC (2001). Dendritic mechanisms of phase precession in hippocampal CA1 pyramidal neurons. *J Neurophysiol* **86**, 528–532.

Mainen ZF & Sejnowski TJ (1995). Reliability of spike timing in neocortical neurons. *Science* **268**, 1503–1506.

Margrie T & Schaefer A (2003). Theta oscillation coupled spike latencies yield computational vigour in a mammalian sensory system. *J Physiol* **546**, 363–374.

Mehta MR, Lee AK & Wilson MA (2002). Role of experience and oscillations in transforming a rate code into a temporal code. *Nature* **417**, 741–746.

Ng B & Barry PH (1995). The measurement of ionic conductivities and mobilities of certain less common organic ions needed for junction potential corrections in electrophysiology. *J Neurosci Methods* **56**, 37–41.

O'Keefe J & Recce ML (1993). Phase relationship between hippocampal place units and the EEG theta-rhythm. *Hippocampus* **3**, 317–330.

Panzeri S, Senatore R, Montemurro MA & Petersen RS (2007). Correcting for the sampling bias problem in spike train information measures. *J Neurophysiol* **98**, 1064–1072.

Pike FG, Goddard RS, Suckling JM, Ganter P, Kasthuri N & Paulsen O (2000). Distinct frequency preferences of different types of rat hippocampal neurones in response to oscillatory input currents. *J Physiol* **529**, 205–213.

Rapoport A & Horvarth WJ (1960). The theoretical channel capacity of a single neuron as determined by various coding schemes. *Inf Control* **3**, 335–350.

Rieke F, Warland D, de Ruyter van Steveninck R & Bialek W (1997). *Spikes: Exploring the Neural Code*. The MIT Press, Cambridge, MA, USA.

Schaefer A, Angelo K, Spors H & Margrie T (2006). Neuronal oscillations enhance stimulus discrimination by ensuring action potential precision. *PLoS Biol* **4**, e163.

Shannon CE (1948). A mathematical theory of communication. *Bell System Techn J* **27**, 379–423.

Skaggs WE, McNaughton BL, Wilson MA & Barnes CA (1996). Theta phase precession in hippocampal neuronal populations and the compression of temporal sequences. *Hippocampus* **6**, 149–172.

Soltesz I & Deschênes M (1993). Low- and high-frequency membrane potential oscillations during theta activity in CA1 and CA3 pyramidal neurons of the rat hippocampus under ketamine-xylazine anesthesia. *J Neurophysiol* **70**, 97–116.

Stein RB (1967). The information capacity of nerve cells using a frequency code. *Biophys J* **7**, 797–826.

Thorpe S, Delorme A & Van Rullen R (2001). Spike-based strategies for rapid processing. *Neural Netw* **14**, 715–725.

Thorpe S & Gautrais J (1998). Rank order coding. In *Computational Neuroscience: Trends in Research*, ed. Bower JM, pp. 113–118. Plenum Press, New York.

Tiesinga PHE, Fellous JM, José JV & Sejnowski TJ (2002). Information transfer in entrained cortical neurons. *Network* **13**, 41–66.

Williams SR (2004). Spatial compartmentalization and functional impact of conductance in pyramidal neurons. *Nat Neurosci* **7**, 961–967.

Yamaguchi Y, Aota Y, McNaughton BL & Lipa P (2002). Bimodality of theta phase precession in hippocampal place cells in freely running rats. *J Neurophysiol* **87**, 2629–2642.

Acknowledgements

This work was supported by the Wellcome Trust.